Baltic Astronomy, vol. 14, 577–591, 2005.

A NEW MODEL FOR THE MULTIPLICITY FUNCTION

A. Del Popolo[1,2,3]

[1] *Boğaziçi University, 80185 Bebek, Istanbul, Turkey*

[2] *Istanbul Technical University, Faculty of Science, Ayazaga Campus, 34469 Maslak, Istanbul, Turkey*

[3] *Dipartimento di Matematica, Università Statale di Bergamo, Piazza Rosate 2, I-24129, Bergamo, Italy*

Received 2005 May 18; revised 2005 August 20

Abstract. An improved theoretical multiplicity function by means of the excursion set approach is found. The barrier shape used implicitly takes into account the total angular momentum acquired by the proto-structure during evolution and the non-zero cosmological constant. The theoretical multiplicity function obtained in the present paper is compared with analytical and numerical multiplicity functions of other authors. It is shown that when one takes into account the total angular momentum, acquired by the proto-structure during evolution, the multiplicity function obtained is in a better agreement with Yahagi, Nagashima & Yoshii (2004) simulations than with the results of other previous models. Differently from some previous multiplicity function models, the theoretical mass function of the present paper is obtained from a sound theoretical background and not by a simple numerical fit. However, the current level of disagreement between different simulations is not sufficient to favor one mass function over another when the differences are at the 10 percent level. Hence, at the present time all of these mass functions are essentially equivalent.

Key words: cosmology: theory – large scale structure of universe – galaxies: formation

1. INTRODUCTION

The study of structure formation is based on semi-analytical models like the Press-Schechter (Press & Schechter 1974, hereafter PS) approach and its extensions (EPS), which are of great interest since they allow us to compute mass functions (PS; Bond et al. 1991), to approximate merging histories (Lacey & Cole 1993, hereafter LC93; Bower 1991; Sheth & Lemson 1999b) and to estimate the spatial clustering of dark matter haloes (Mo & White 1996; Catelan et al. 1998; Sheth & Lemson 1999a). Another technique used is based on N-body simulations, that are able to follow the evolution of a large number of particles under the influence of the mutual gravity, from initial conditions to the present epoch. It is well known that the PS mass function, while qualitatively correct, disagrees with the results of N-body simulations even if the PS model is refined (Bond et al. 1991; Lacey & Cole 1993). A better agreement between the numerical mass function and the analytic mass function can be obtained by incorporating into the PS approach the non-sphericity of collapse model (Del Popolo & Gambera 1998; Sheth & Tormen 1999, hereafter ST; Sheth, Mo & Tormen 2001, hereafter SMT; Sheth & Tormen 2002, hereafter ST1; Jenkins et al. 2001, hereafter J01), instead of the spherical model, or taking into account the spatial correlation of density fluctuations (Nagashima 2001).

More recently, Yahagi, Nagashima & Yoshii (2004, hereafter YNY) showed that discrepancies are observed between some of the quoted analytical multiplicity functions with high mass resolution simulations: for example the maximum value of the multiplicity function from their simulations at $\nu \simeq 1$ is smaller, and its low mass tail is shallower when compared with the ST, ST1 multiplicity function. As previously reported, multiplicity functions like ST and J01, fit only approximately high resolution N-body simulations like those of YNY, while the functional form proposed in YNY, provides a better fit (as shown by a χ^2 fit) when compared with the ST functional form. Unfortunately, the functional form for the multiplicity function proposed in YNY and similarly that of J01 (which is a fit to their "Hubble Volume" simulations of τCDM and ΛCDM cosmologies) are not based on any theoretical background. So it is important to find a better analytical form, which starting by "first principles" is able to fit in a better way simulations and is physically motivated. In the present paper, I use an improved version of the barrier shape obtained in Del Popolo & Gambera (1998), which takes into account the effects of asphericity and tidal interaction between protohalos and the effects of a non-zero cosmological constant, together with the results of ST, ST1. I show that the function obtained in the present paper, similarly to that in YNY, provides a better fit than the ST or other functional forms used in the literature and, moreover, it has been obtained from solid physical theoretical arguments.

However, while the theoretical mass function of the present paper agrees with YNY it does not agree with another recent simulation, namely, that of Reed et al. (2003, hereafter R03). This discrepancy shows that it is premature to favor one mass function over another, since the differences among them are at the 10 percent level. Hence, from the point of view of describing simulations, at the present time all of these mass functions are essentially equivalent.

The paper is organized as follows: in Section 2 I calculate the "unconditional" multiplicity function, Sections 3 and 4 are devoted to results and to conclusions, respectively.

2. THE MULTIPLICITY FUNCTION AND THE MOVING BARRIER MODEL

According to hierarchical scenarios of structure formation, a region collapses at time t if its overdensity at that time exceeds some threshold. The linear extrapolation of this threshold up to the present time is called a barrier, B. A likely form of this barrier is (ST, ST1):

$$B(\sigma^2, z) = \sqrt{aS_*}\left[1 + \beta\,(S/aS_*)^\alpha\right] = \sqrt{a}\delta_c(z)\left[1 + \frac{\beta}{(a\nu)^\alpha}\right]. \quad (1)$$

In the above equation a, β and α are constants, $S_* = \delta_c^2$, where $\delta_c(t)$ is the linear extrapolation up to the present-day of the initial overdensity of a spherically symmetrical region, that collapsed at time t. Additionally, $S \equiv S_*\left(\frac{\sigma}{\sigma_*}\right)^2 = \frac{S_*}{\nu}$, $\sigma_* = \sqrt{S_*} = \delta_{co}$, $\nu = \left(\frac{\delta_c(t)}{\sigma(M)}\right)^2$, where $\sigma^2(M)$ is the present-day mass dispersion on comoving scale containing mass M. S depends on the assumed power spectrum.

The spherical collapse model (SC) has a barrier that does not depend on the mass (e.g., Lacey & Cole 1993, hereafter LC93). For this model the values of the parameters are $a = 1$ and $\beta = 0$. The ellipsoidal collapse model (EC) of ST has a barrier that depends on the mass (moving barrier). The values of the parameters are $a = 0.707$, $\beta = 0.485$, $\gamma = 0.615$ and are adopted either from the dynamics of ellipsoidal collapse or from fits to the results of N-body simulations.

In the following, I shall use an improved version of the barrier obtained in Del Popolo & Gambera (1998) to get the mass functions, which will be compared with those obtained by PS, ST, J01, YNY, and with numerical simulations of YNY and R03. Since the way the barrier is obtained is described in previous papers (see Del Popolo & Gambera 1998, 1999, 2000) the reader is referred to those papers for details. Assuming that the barrier is proportional to the threshold for the collapse, similarly to ST, the barrier can be expressed, in the case of a zero cosmological constant, in the form:

$$B(M) = \delta_{\rm c}(\nu, z) = \delta_{\rm co}\left[1 + \int_{r_{\rm i}}^{r_{\rm ta}} \frac{r_{\rm ta} L^2 \cdot {\rm d}r}{GM^3 r^3}\right] \simeq \delta_{\rm co}\left[1 + \frac{\beta_1}{\nu^{\alpha_1}}\right], \tag{2}$$

where $\delta_{\rm co} = 1.68$ is the critical threshold for a spherical model, $r_{\rm i}$ is the initial radius, $r_{\rm ta}$ is the turn-around radius, L is the angular momentum, $\alpha_1 = 0.585$ and $\beta_1 = 0.46$. The angular momentum appearing in Eq. (2) is the total angular momentum acquired by the proto-structure during evolution. In order to calculate L, I will use the same model as described in Del Popolo & Gambera (1998, 1999) (more hints on the model and some of the model limits can be found in Del Popolo, Ercan & Gambera 2001).

Assuming a non-zero cosmological constant Eq. (1) is changed as follows (see Appendix):

$$B(M) = \delta_{\rm c}(\nu, z) = \delta_{\rm co}\left[1 + \int_{r_{\rm i}}^{r_{\rm ta}} \frac{r_{\rm ta} L^2 \cdot {\rm d}r}{GM^3 r^3} + \Lambda\frac{r_{\rm ta} r^2}{6GM}\right] \simeq \delta_{\rm co}\left[1 + \frac{\beta_1}{\nu^{\alpha_1}} + \frac{\Omega_\Lambda \beta_2}{\nu^{\alpha_2}}\right], \tag{3}$$

where $\alpha_2 = 0.4$ and $\beta_2 = 0.02$ and Ω_Λ is the contribution to the density parameter coming from the cosmological constant. ST1 connected the form of the barrier with the form of the multiplicity function. As shown by ST1, for a given barrier shape, $B(S)$, the first crossing distribution is well approximated by:

$$f(S)dS = |T(S)| \exp(-\frac{B(S)^2}{2S})\frac{dS/S}{\sqrt{2\pi S}}, \tag{4}$$

where $T(S)$ is the sum of the first few terms in the Taylor expansion of $B(S)$:

$$T(S) = \sum_{n=0}^{5} \frac{(-S)^n}{n!} \frac{\partial^n B(S)}{\partial S^n}. \tag{5}$$

In the case of the ellipsoidal barrier shape given in ST (Eq. (1) of the present paper), Eqs. (4) and (5), after truncating the expansion at $n = 5$ (see ST), give:

$$\nu f(\nu) = \sqrt{a\nu/2\pi}[1 + \beta(a\nu)^{-\alpha} g(\alpha)] \exp\left(-0.5a\nu[1 + \beta(a\nu)^{-\alpha}]^2\right), \tag{6}$$

where

$$g(\alpha) = |\, 1 - \alpha + \frac{\alpha(\alpha-1)}{2!} - ... - \frac{\alpha(\alpha-1)\cdots(\alpha-4)}{5!}\,| \,. \tag{7}$$

Using the values for β and α of ST ($a = 0.707$, $\delta_c(z) = 1.686(1+z)$, $\beta \simeq 0.485$ and $\alpha \simeq 0.615$) in Eq. (6) I get (ST1):

$$\nu f(\nu) \simeq A_1 \left(1 + \frac{0.094}{(a\nu)^{0.6}}\right) \sqrt{\frac{a\nu}{2\pi}} \exp\{-a\nu \left[1 + \frac{0.5}{(a\nu)^{0.6}}\right]^2 /2\} \tag{8}$$

with $A_1 \simeq 1$. This last result is in good agreement with the fit of the simulated first-crossing distribution (ST):

$$\nu f(\nu) = A_2 \left(1 + \frac{1}{(a\nu)^p}\right) \sqrt{\frac{a\nu}{2\pi}} \exp(-a\nu/2), \tag{9}$$

where $p = 0.3$ and $a = 0.707$.

The normalization factor A_2 has to satisfy the constraint:

$$\int_0^\infty f(\nu) d\nu = 1 \tag{10}$$

and as a consequence it is not an independent parameter, but is expressed in the form:

$$A_2 = \left[1 + 2^{-p}\pi^{-1/2}\Gamma(1/2 - p)\right]^{-1} = 0.3222. \tag{11}$$

In the case of the barrier given in Eq. (2), the "unconditional" multiplicity function can be approximated by:

$$\nu f(\nu) \simeq A_3 \left(1 + \frac{b}{(a\nu)^{0.585}}\right) \sqrt{\frac{a\nu}{2\pi}} \exp\{-ac\nu \left[1 + \frac{d}{(a\nu)^{0.585}}\right]^2\}, \tag{12}$$

where $a = 0.707$, $b = 0.1218$, $c = 0.4019$, $d = 0.5526$ and $A_4 \simeq 1.75$ is obtained from the normalization condition.

If the barrier takes account of the cosmological constant, like in Eq. (3), using the same method that lead to Eq. (6), we have that:

$$\nu f(\nu) = A_4 \left(1 + \frac{\beta_1 g(\alpha_1)}{(a\nu)^{\alpha_1}} + \frac{\beta_2 g(\alpha_2)}{(a\nu)^{\alpha_2}}\right) \sqrt{\frac{a\nu}{2\pi}} \exp\{-a\nu \left[1 + \frac{\beta_1}{(a\nu)^{\alpha_1}} + \frac{\beta_2}{(a\nu)^{\alpha_2}}\right]^2 /2\}. \tag{13}$$

In the case of the barrier with a non-zero cosmological constant, Eq. (3), a good approximation to the multiplicity function is given by:

$$\nu f(\nu) \simeq A_5 \left(1 + \frac{0.1218}{(a\nu)^{0.585}} + \frac{0.0079}{(a\nu)^{0.4}}\right) \sqrt{\frac{a\nu}{2\pi}} \exp\{-0.4019 a\nu \left[1 + \frac{0.5526}{(a\nu)^{0.585}} + \frac{0.02}{(a\nu)^{0.4}}\right]^2\}, \tag{14}$$

where $A_5 = 1.75$.

As previously reported, for the matter of completeness, to the previous functions, namely PS, ST, Eq. (14), we have to add J01, which satisfies the equation:

$$\begin{aligned} \nu f(\nu) &= 0.315 \exp(- \mid 0.61 + \ln[\sigma^{-1}(M)] \mid^{3.8}) = \\ & \quad 0.315 \exp(- \mid 0.61 + \ln \sqrt{\nu} - \ln \delta_c \mid^{3.8}). \end{aligned} \tag{15}$$

The above formula is valid for $-1.2 < \ln \sqrt{\nu} - \ln \delta_c < 1.05$.

YNY (Eq. 7, hereafter YNY7) proposed the following function to fit the numerical multiplicity function:

$$\nu f(\nu) = A_6[1 + (B\sqrt{\nu})/\sqrt{2})^C]\sqrt{\nu}^D \exp[-(B\sqrt{\nu}/\sqrt{2})^2], \tag{16}$$

where A_6 is a normalization factor to satisfy the unity constraint, $\int_0^\infty f(\nu)d\nu = 1$, therefore

$$A_6 = 2(B/\sqrt{2})^D \{\Gamma[D/2] + \Gamma[(C+D)/2]\}^{-1}. \tag{17}$$

The best-fit parameters are given as B=0.893, C=1.39 and D=0.408, and from these parameters A is constrained so that $A_6 = 0.298$.

The CDM spectrum used in the present paper is that of Bardeen et al. (1986) (equation (G3)). The power spectrum was normalized to reproduce the observed abundance of rich cluster of galaxies (e.g., Bahcal & Fan 1998). In the simulations, the same BBKS power spectrum was used.

3. RESULTS AND DISCUSSION

In this section, I compare the analytic multiplicity functions of PS, ST, J01, YNY7 and Eq. (14) of the present paper, with the numerical simulations of YNY and R03. Those simulations adopt the ΛCDM cosmological parameters of $\Omega_m = 0.3$, $\Omega_\lambda = 0.7$, $h = 0.7$ and $\sigma_8 = 1.0$, using 512^3 particles in common (see YNY for details). The comparison between numerical multiplicity functions and theoretical ones is shown in Figure 1. In the plot the short-dashed line represents the multiplicity function obtained in the present paper, the solid line – YNY7, the dot-dashed line – the ST multiplicity function, the long-dashed line – the J01 multiplicity function. The error bars with open circles represent the run 140 of YNY, those with filled squares – the case 70b, those with open squares – the case 70a, those with filled circles – the case 35b, those with crosses – the case 35a. Since the data are available only in the region at $\nu \leq 3$, these functions could be erroneous at $\nu \geq 3$. Note that the comparison of the above curves, except for the PS model, with the results of N-body simulations show a very good agreement. However, there are some discrepancies between the YNY multiplicity function and other model functions (except this in the present paper). First, the multiplicity function of the present paper, similarly to that of YNY, in the low-ν region of $\nu \leq 1$, systematically falls below the ST and the J01 functions. In this region the multiplicity function of the present paper is very close to that of YNY. As seen in Figure 1, and in agreement with YNY, the numerical multiplicity functions reside between the ST and J01 multiplicity functions at $2 \leq \nu \leq 3$ (except for the run 35b). Additionally, the numerical multiplicity functions have an apparent peak at $\nu \sim 1$ instead of the plateau that is seen in the J01 function. On the other hand, in the high-ν region, where ν is significantly larger than unity, the multiplicity function of the present paper like YNY takes values between ST and J01 functions. These differences between numerical multiplicity functions and analytic ones, like ST, ST1 and J01, are within 1 σ error bars, and they are possibly due to the different box sizes adopted (see YNY for a discussion). To be more precise, throughout the peak range of $0.3 \leq \nu \leq 3$, the ST multiplicity function is in disagreement with the high mass resolution N-body simulations of YNY and that of the present paper. As shown by YNY, the ST functional form provides a good fit to them only choosing parameter values of $a = 0.664, p = 0.321$ and $A_2 = 0.301$. The multiplicity function obtained in the present paper has a peak at $\nu \sim 1$ as in the ST function, and YNY numerical multiplicity function and YNY7, instead of a plateau as in the J01 function.

I want to stress that the functional form proposed in YNY, namely YNY7, provides a better fit when compared with the ST functional form but it is not based on theoretical background. The function obtained in the present paper, similarly to YNY7 provides a better fit to simulations than the ST functional form, and at the same time it has been obtained from solid physical, theoretical arguments. The better agreement observed between the multiplicity function of the present paper and YNY simulations, when compared with the ST, is connected to the shape of the barrier (δ_c). Taking into account the effects of asphericity and tidal interaction with neighbors, Del Popolo & Gambera (1998), showed that the threshold is mass-dependent, and in particular that of the set of objects that collapse at the same time, the less massive ones must initially have been denser than the more massive, since the less massive ones would have had to hold themselves together against stronger tidal forces.

The shape of the barrier given in Eq. (2) is a direct consequence of the angular momentum acquired by the proto-structure during evolution while Eq. (3) introduces the effects of the cosmological constant. Similarly to ST, the barrier increases with S (decrease with mass, M) differently than in other models (see Monaco 1997a,b). It is interesting to note that the increase of the barrier with S has several important consequences, and these models have a richer structure than the constant barrier model.

The decrease of the barrier with mass means that, in order to form structure, more massive peaks must cross a lower threshold, $\delta_c(\nu, z)$, with respect to under-dense ones. At the same time, since the probability to find high peaks is larger in more dense regions, this means that, statistically, in order to form structure, peaks in more dense regions may have a lower value of the threshold, $\delta_c(\nu, z)$, with respect to those of under-dense regions. This is due to the fact that less massive objects are more influenced by external tides, and consequently they must be more overdense to collapse by a given time. In fact, the angular momentum acquired by a shell centered on a peak in the CDM density distribution is anti-correlated with density: high-density peaks acquire less angular momentum than low-density peaks (Hoffman 1986; Ryden 1988). A larger amount of angular momentum acquired by low-density peaks (with respect to the high-density ones) implies that these peaks can more easily resist gravitational collapse and, consequently, it is more difficult for them to form structure. Therefore, on small scales, where the shear is statistically greater, structures need, on average, a higher density contrast to collapse.

It is evident that the effect of a non-zero cosmological constant adds to that of L. The effect of a non-zero cosmological constant is that of slightly changing the evolution of the multiplicity function with respect to open models with the same

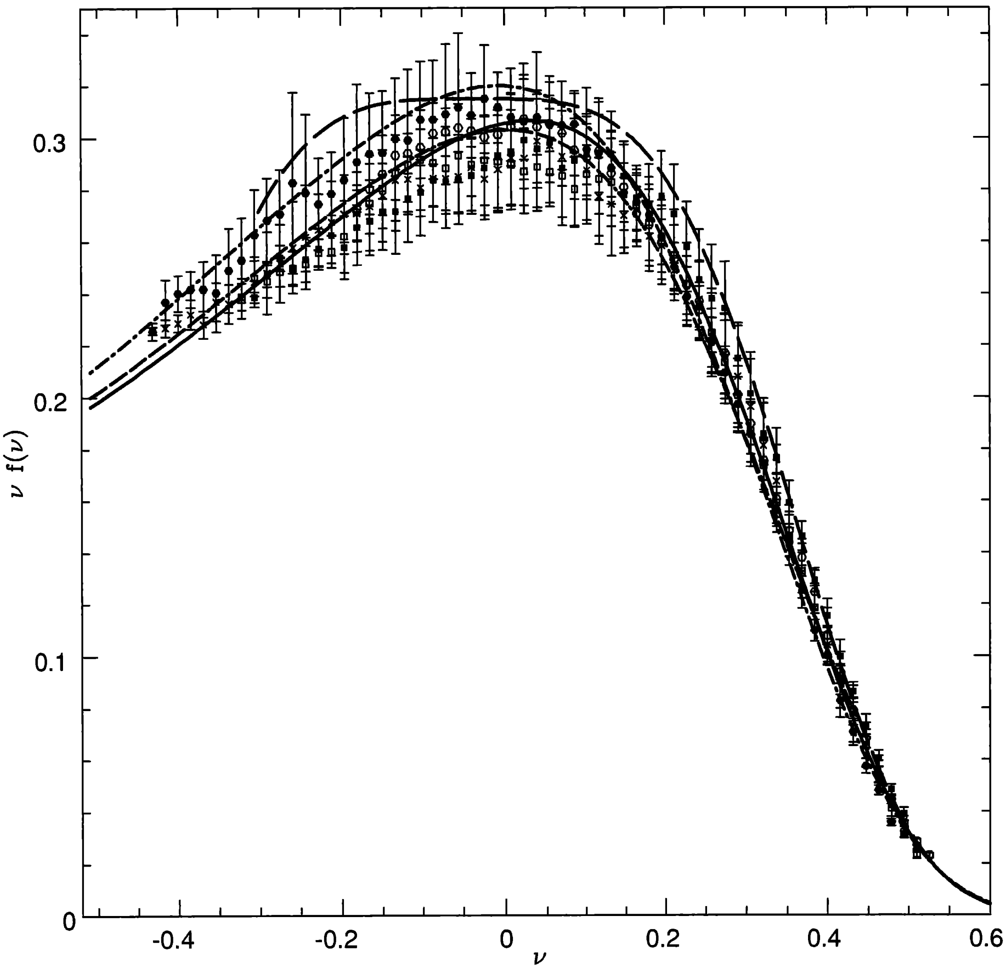

Fig. 1. The best-fit multiplicity function. In the plot the short-dashed solid line represents the multiplicity function obtained in the present paper, the solid line – YNY7, the dot-dashed line – the ST multiplicity function, the long-dashed line – the J01 multiplicity function. The error bars with open circles represent the run 140 of YNY, those with filled squares – the case 70b, those with open squares – the case 70a, those with filled circles – the case 35b, those with crosses – the case 35a.

value of Ω_0. This is caused by the fact that in a flat universe with $\Omega_\Lambda > 0$, the density of the universe remains close to the critical value later in time, promoting perturbation growth at lower redshift. The evolution is more rapid for larger values (in absolute value) of the spectral index, n.

As previously reported, the ST model gives a better fit to simulations than PS model, but it has some discrepancies with simulations. The ST model was introduced at the beginning (Sheth & Tormen 1999) as a fit to the GIF simulations, and in a subsequent paper (SMT) the importance of aspherical collapse in the functional form of the mass function was recognized. The effects of asphericity were taken into account by changing the functional form of the critical overdensity (barrier) by means of a simple intuitive parametrization of elliptical collapse of isolated

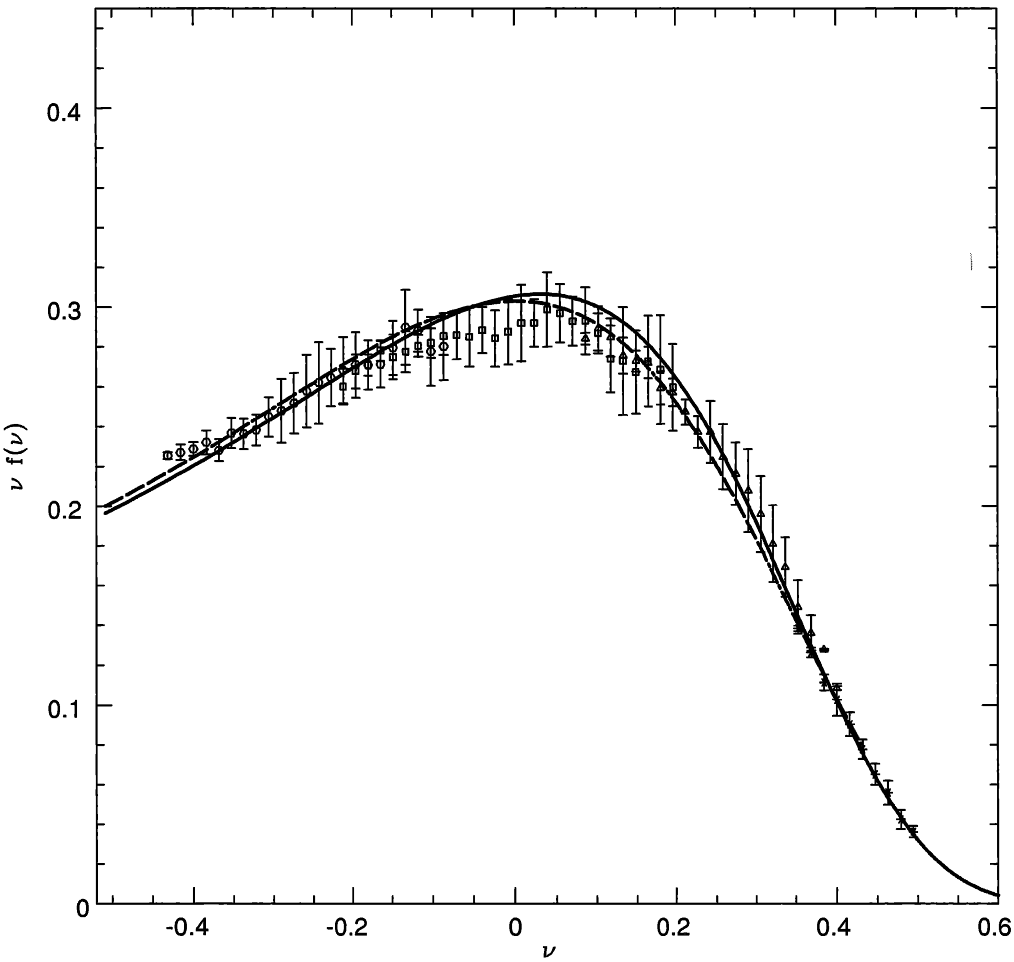

Fig. 2. Time-dependence of the multiplicity function from the 35a run, for four redshift ranges of $0 \leq z < 1$ (open circles), $1 \leq z < 3$ (open squares), $3 \leq z < 6$ (open triangles), and $z \geq 6$, (crosses). Also shown are YNY7 (solid line) and the model of the present paper (short-dashed line).

spheroids. The model proposed in the present paper has several similarities with the ST and ST1 models, namely it uses the excursion set approach as extended by ST1 to calculate the multiplicity function, but at the same time it differs from ST and ST1 for the way the barrier was calculated and for the fact that it takes into account the angular momentum acquisition, which is not accounted by ST and ST1. These differences gives rise to a multiplicity function in a better agreement with simulations. This shows the importance of the form of the barrier.

In other words, the excursion set approach with a barrier taking account effects of physics of the structure formation gives rise to good approximations to the numerical multiplicity function: the approximation goodness increases with a more improved form of the barrier (taking account more and more physical effects: angular momentum acquisition, non-zero cosmological constant, etc.). Another important aspect of the quoted method is its noteworthy versatility: for example it is very easy to take account of the presence of a non-zero cosmological constant

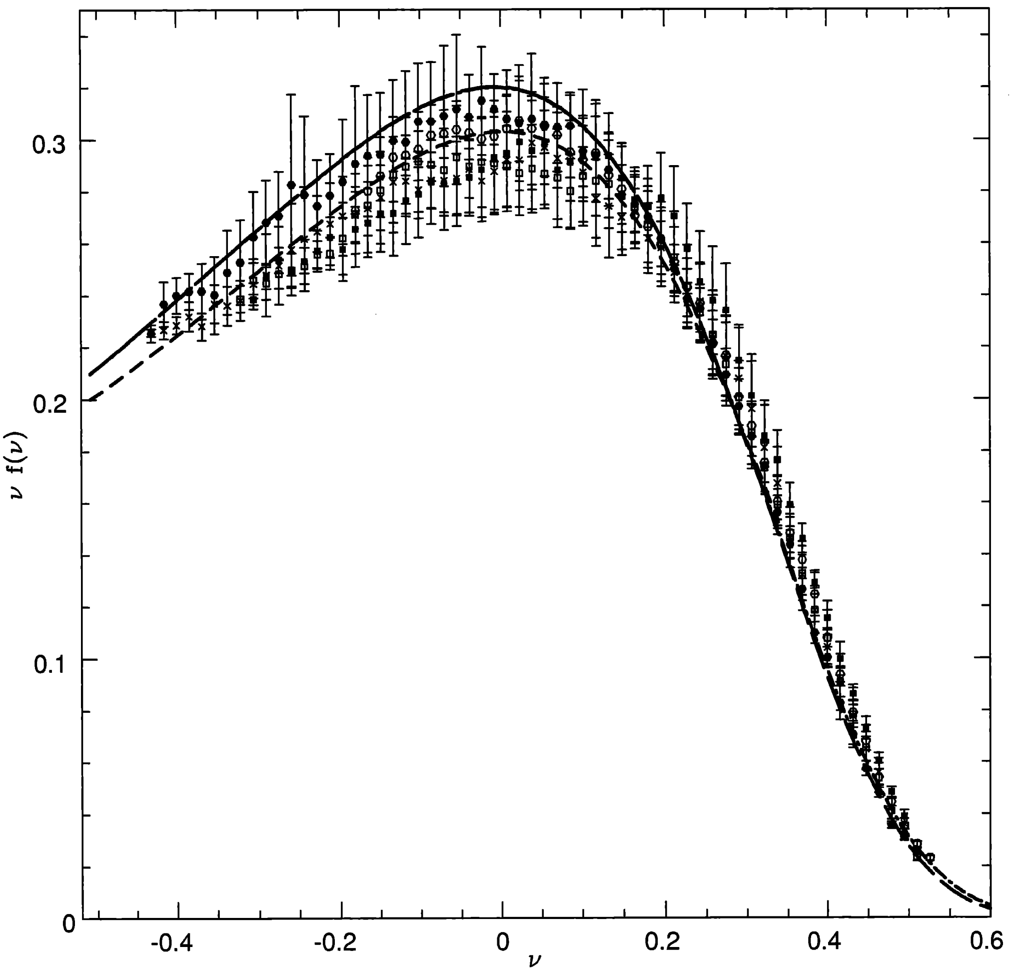

Fig. 3. The same as in Figure 1 but here the plot is only for the ST multiplicity function (dot-dashed line in Fig. 1, solid line here) with superimposed the R03 result (long-dashed line).

englobing it in the barrier.

Then I checked the time dependence of the multiplicity function. Figure 2 shows the multiplicity function from the 35a run for four redshift ranges of $0 \leq z < 1$ (open circles), $1 \leq z < 3$ (open squares), $3 \leq z < 6$ (open triangles) and $z \geq 6$ (crosses). At high redshifts, high-ν halos in the exponential part of the YNY7 (solid line) function and Eq. (14) (short-dashed line of the present paper) are probed. As redshift decreases, the probe window moves to the lower-ν region. Figure 2 shows that the multiplicity function of this paper, Eq. (14), and YNY7 both gives a good fit to the numerical simulations. For small values of ν, Eq. (14) gives a slightly better fit to the data, and at large values of ν the two functions decay in the same way.

R03 used a high resolution ΛCDM numerical simulation to calculate the mass function of dark matter haloes down to the scale of dwarf galaxies, back to a redshift of 15, in a 50 h^{-1} Mpc volume containing 80 million particles. Their low redshift results allow us to probe low σ density fluctuations significantly beyond the

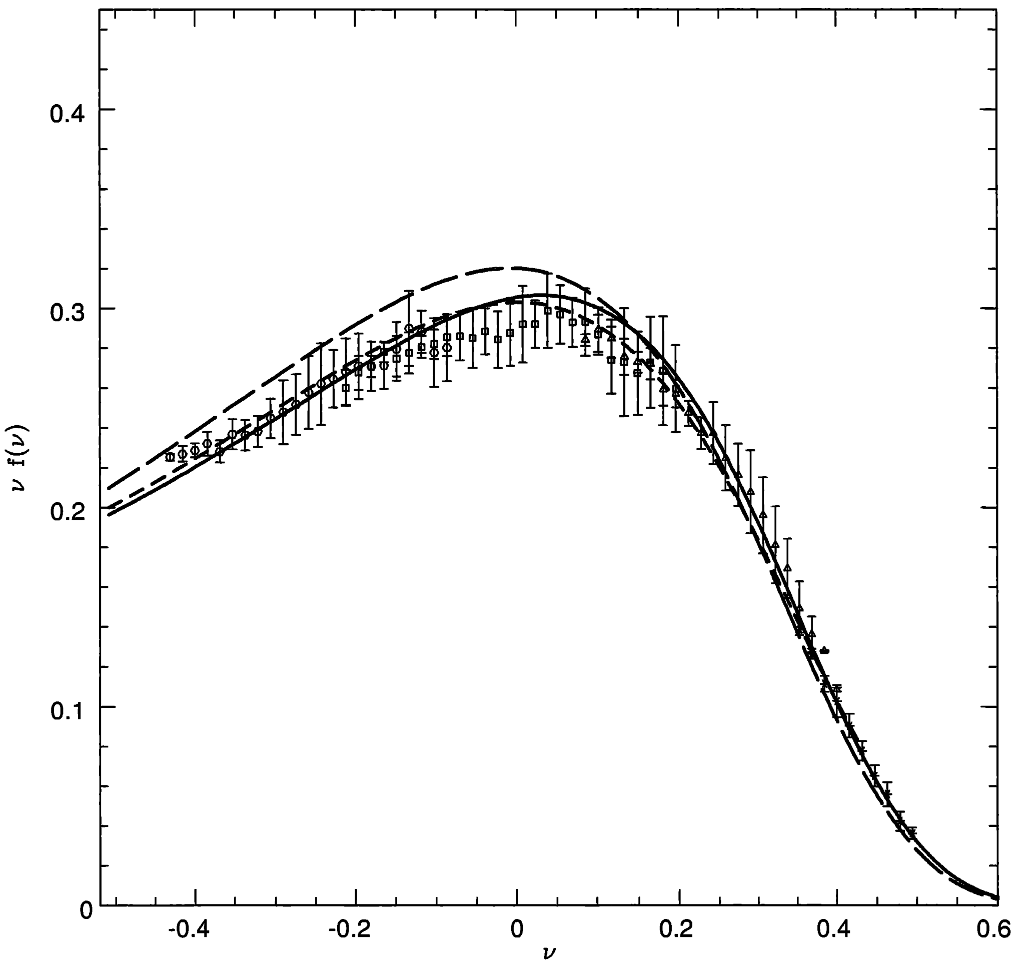

Fig. 4. The same as in Fig. 2 but here the result of R03 (long-dashed line) is also plotted.

range of previous cosmological simulations. They also considered the possibility of an empirical adjustment to the ST function. They inserted a crude multiplicative factor to the ST function as follows:

$$f(\sigma) = f(\sigma;\mathrm{ST})\left[\exp[-0.7/(\sigma[\cosh(2\sigma)]^5)]\right], \tag{18}$$

valid over the range of $-1.7 \leq \ln\sigma^{-1} \leq 0.9$. The resulting function is virtually identical to the ST function for all $-\infty \leq \ln\sigma \leq 0.4$. At higher values of $\ln\sigma^{-1}$, this function declines relative to the ST function, reflecting an underabundance of haloes that becomes greater with increasing $\ln\sigma^{-1}$. For $-1.7 \leq \ln\sigma^{-1} \leq 0.5$, Eq. (18) matches Reed's et al. (2003) data to better than 10% for well-sampled bins, while for $0.5 \leq \ln\sigma^{-1} \leq 0.9$, where Poisson errors are larger, the data are matched to roughly 20%.

In Figures 3 and 4 the result of R03 is compared with Figures 1 and 2, respectively. Figure 3 is the same as Figure 1 but now I plot only the ST multiplicity function (solid line) with the superimposed R03 result (long-dashed line). As shown the two curves coincide except for the tail at the right, where the R03 lies under the ST. The short-dashed line represents the multiplicity function obtained in the present paper. Figure 4 is the same as Figure 2 but now I also plot the result of R03 (long-dashed line).

An important point to be discussed here is that in the YNY simulations; the simulation volume is smaller when compared with that of other studies. As previously reported, R03 used a high resolution ΛCDM numerical simulation to calculate the mass function of dark matter haloes. They showed that the ST function provides a good fit to their simulation with excellent agreement at all masses and redshifts except for the highest redshift outputs, where it significantly overpredicts the halo abundance.

Figures 3 and 4 compare the result of R03 with that of the present paper and YNY. The R03 results are in a very good agreement with ST for almost all ν range except for high value of ν where Reed's mass function is lower than the ST fit. At the same time the R03 results are compatible with YNY simulations and they only give a smaller value of the multiplicity function for high value of ν (in the range not tested by YNY). A larger discrepancy between the R03 result and YNY is seen in Figure 4.

It is important to try to understand to what this last discrepancy is due. In fact, the R03 box is comparable to some of the YNY boxes (i.e. relatively small), and yet, their best fit differs from that given by YNY. In fact, the difference between R03 fit and that given by YNY is similar in magnitude to the difference between J01 or ST, and the fit proposed in this paper.

In the determination of the numerical mass function several factors are important: resolution, box-size, cluster finding algorithm adopted. Previous papers in the literature (Gelb & Bertschinger 1994; Governato et al. 1999; Lacey & Cole 1993), showed that the numerical mass function depends on the cluster finding algorithm adopted. J01 demonstrated that the friends-of-friends (FoF) algorithm (Davis et al. 1985) with a fixed linking length of 0.2 times the mean particle separation results in the numerical mass function that shows the best universality for various compositions of cosmological parameters and box sizes. White (2002, hereafter W02) supported the above argument and demonstrated that another definition of mass of halos, M_{180}, gives the universal numerical mass function.

Summarizing, the changes on the quoted simulation parameters and the way objects are identified lead to different results. In other words, even the numerical multiplicity function can be improved, as shown by the improvements obtained in the last decade: for example, even in YNY there is a discrepancy in the numerical multiplicity functions from various simulation runs, which can be solved by means of different strategies: (a) running simulations having still higher mass dynamic range free from the box size effect; (b) increasing the number of realizations as W02 did, because there is a scatter from the runs using the same box size; (c) running simulations whose box size is smaller than that of the present work, although it might sound contradictory.

In the particular case of YNY, they used the Adaptive Mesh Refinement N-body code developed by Yahagi (2002), which is a vectorized and parallelized version of the code described in Yahagi & Yoshii (2001). As previously reported, the simulations adopt the ΛCDM cosmological parameters of $\Omega_m = 0.3$, $\Omega_\lambda = 0.7$, $h = 0.7$ and $\sigma_8 = 1.0$, using 512^3 particles in common. The size of the finest mesh is 1/64 of the base mesh, and the force dynamic range is $2^{15} = 32768$. Other simulation parameters, such as the box size and the particle mass, are given in Table 1 of YNY. As an example, the run 35a has a box size $L = 35h^{-1}$ Mpc, a particle mass of $2.67 \times 10^7 h^{-1} M_\odot$ and the initial redshift $z_{\rm start} = 50$. The results of the simulations were analyzed by the FoF algorithm with a constant linking length of 0.2 times the mean particle separation.

In the case of R03, the simulations adopt, as in R03, the presently favored ΛCDM with $\Omega_\lambda = 0.7$ and $\Omega_m = 0.3$. They use the parallel tree gravity solver PKDGRAV (Stadel 2001) to simulate 81×10^6 (432^3) dark matter particles from a starting redshift, $z_{\rm start}$, of 69. Then, they re-simulate the same volume but with $z_{\rm start} = 139$, and evolve this volume to $z = 7$, which allows to consider results at higher redshift than with the $z_{\rm start} = 69$ run. In order to simulate the highest possible mass resolution, they employ a volume of 50 h^{-1} Mpc on a side. The particle mass is $1.3 \times 10^8 h^{-1} M_\odot$ allowing a haloes resolution down to less than $10^{10} h^{-1} M_\odot$ with 75 particles. The force resolution is 5 h^{-1} kpc. The authors use a cell opening angle of $\Theta < 0.8$ at low redshift, and $\Theta < 0.7$ at $z > 2$. They use a "multistepping" approach, where particles in the highest density regions undergo 16 000 time steps. In order to identify haloes in their simulation, both the FoF algorithm (Davis et al. 1985) and the SO (spherical overdensity) algorithm (Lacey & Cole 1994) were used. The different parameter choice in the two N-body simulations, namely YNY and R03, are most probably the cause in the difference in the mass function.

In the light of the previous discussion, perhaps it is premature to make strong statements about which theoretical mass function provides a better fit, since even the simulations themselves have not reached agreement on the correct shape of the mass function. Hence, from the point of view of describing simulations, at the present time all of these mass functions are essentially equivalent.

In any case, when one takes account of total angular momentum acquired by the proto-structure during evolution and of a non-zero cosmological constant, the theoretical mass function obtained is in better agreement with that of YNY simulations than with other previous models (Sheth & Tormen 1999; Sheth, Mo & Tormen 2001; Sheth & Tormen 2002; Jenkins et al. 2001). Moreover, differently from other theoretical mass functions, the one of the present paper was obtained from a sound theoretical background.

4. CONCLUSIONS

In the present paper the numerical multiplicity function given in YNY is compared with the theoretical multiplicity function obtained by means of the excursion set model and an improved version of the barrier shape obtained in Del Popolo & Gambera (1998), which implicitly takes account of tidal interactions between clusters and a non-zero cosmological constant. I show that the barrier obtained in Del Popolo & Gambera (1998) gives rise to a better description of the multiplicity functions than other models (ST, J01), and the agreement is based on sound theoretical models and not on fitting to simulations.

The main results of the paper can be summarized as follows.

(1) the non-constant barrier of the present paper combined with the ST1 model gives "unconditional" multiplicity functions in a better agreement with the N-body simulations of YNY than with other previous models (ST, ST1, J01).

(2) The comparison of the theoretical multiplicity function of the present paper,

in agreement with the YNY result, shows some discrepancies with the theoretical multiplicity functions of several authors (ST, ST1, J01): e.g., the maximum value of the multiplicity function from simulations at $\nu \sim 1$ is smaller, and its low mass tail is shallower when compared with the ST multiplicity function.

(3) The multiplicity function of the present paper gives a good fit to simulations results as the fit function proposed by YNY, but differently from that it was obtained from a sound theoretical background.

(4) While the theoretical mass function of the present paper agrees with YNY, it does not agree with another recent simulation, namely that of R03. This discrepancy shows that it is premature to favor one mass function over another, since the differences among them are at the 10 percent level. Hence, from the point of view of describing simulations, at the present time all of these mass functions a equivalent.

(5) The excursion set model with a moving barrier is very versatile since it is very easy to introduce several physical effects in the calculation of the multiplicity function, just modifying the barrier.

The above considerations show that it is possible to get accurate predictions for a number of statistical quantities associated with the formation and clustering of dark matter haloes by incorporating a non-spherical collapse which takes account of a non-zero cosmological constant in the excursion set approach. The improvement is probably connected also to the fact that incorporating the non-spherical collapse with increasing barrier in the excursion set approach results in a model in which fragmentation and mergers may occur. Moreover, the effect of a non-zero cosmological constant adds to the effect of angular momentum slightly changing the evolution of the multiplicity function with respect to open models with the same value of matter density parameter.

REFERENCES

Bahcal N. A., Fan X. 1998, ApJ, 504, 1

Bardeen J. M., Bond J. R., Kaiser N., Szalay A. S. 1986, ApJ, 304, 15

Bond J. R., Cole S., Efsthatiou G., Kaiser N. 1991, ApJ, 379, 440

Bower R. G. 1991, MNRAS, 248, 332

Catelan P., Lucchin F., Matarrese S., Porciani C. 1998, MNRAS, 297, 692

Davis M., Efstathiou G., Frenk C. S., White S. D. M. 1985, ApJ, 292, 371

Del Popolo A. 2002, MNRAS, 336, 8190

Del Popolo A., Ercan E. N., Xia Z. Q. 2001, AJ, 122, 487

Del Popolo A., Gambera M. 1998, A&A, 337, 96

Del Popolo A., Gambera M. 1999, A&A, 344, 17

Del Popolo A., Gambera M. 2000, A&A, 357, 809

Efstathiou G., Frenk C.S., White S.D.M., Davis M., 1988, MNRAS 235, 715

Eisenstein D. J., Loeb A. 1995, ApJ, 439, 520

Gelb J. M., Bertschinger E. 1994, ApJ, 436, 467

Governato F., Babul A., Quinn T., Tozzi P., Baugh C., Katz N., Lake G. 1999, MNRAS, 307, 949

Jenkins A., Frenk C. S., White S. D. M., Colberg J. M., Cole S., Evrard A. E., Couchman H. P. M., Yoshida N. 2001, MNRAS, 321, 372
Hoffman Y. 1986, ApJ, 301, 65
Hoyle F. 1949, in *IAU and International Union of Theorethical and Applied Mechanics Symposium*, p. 195
Lacey C., Cole S. 1993, MNRAS, 262, 627
Lacey C., Cole S. 1994, MNRAS, 271, 676
Mo H. J., White S. D. M. 1996, MNRAS, 282, 347
Monaco P. 1997a, MNRAS, 287, 753
Monaco P. 1997b, MNRAS, 290, 439
Nagashima M., Totani T., Gouda N., Yoshii Y. 2001, ApJ, 557, 505
Peebles P. J. E. 1969, ApJ, 155, 393
Press W. H., Schechter P. 1974, ApJ, 187, 425
Reed D., Gardner J., Quinn T. et al. 2003, MNRAS, 346, 565
Ryden B. S. 1988, ApJ, 329, 589
Sheth R. K., Lemson G. 1999a, MNRAS, 304, 767
Sheth R. K., Lemson G. 1999b, MNRAS, 305, 946
Sheth R. K., Tormen G. 1999, MNRAS, 308, 119
Sheth R. K., Mo H. J., Tormen G. 2001, MNRAS, 323, 1 (SMT)
Sheth R. K., Tormen G. 2002, MNRAS, 329, 61 (ST)
Stadel J. 2001, Ph.D. thesis
Tozzi P., Governato F. 1998, in *The Young Universe: Galaxy Formation and Evolution at Intermediate and High Redshift*, eds. S. D'Odorico, A. Fontana & E. Giallongo, ASP Conf. Ser., 146, 461
White S. D. M. 1984, ApJ, 286, 38
White M. 2002, ApJS, 143, 241
Yahagi H. 2002, Ph.D. thesis, University of Tokyo
Yahagi H., Yoshii Y. 2001, ApJ, 558, 463
Yahagi H., Nagashima M., Yoshii Y. 2004, ApJ, 605, 709

APPENDIX

The equation governing the collapse of a density perturbation taking account angular momentum acquisition by protostructures can be obtained using a model due to Peebles (Peebles 1993) (see also Del Popolo & Gambera 1998, 1999).

Let us consider an ensemble of gravitationally growing mass concentrations and suppose that the material in each system collects within the same potential well with inward pointing acceleration given by $g(r)$ (see Del Popolo & Gambera 1998). We indicate with $dP = f(L, rv_r, t)dLdv_rdr$ the probability that a particle can be found in the proper radius range r, $r + dr$, in the radial velocity range $v_r = \dot{r}$, $v_r + dv_r$ and with angular momentum $L = rv_\theta$ in the range dL. The radial acceleration of the particle is:

$$\frac{dv_r}{dt} = \frac{L^2(r)}{M^2r^3} - g(r) = \frac{L^2(r)}{M^2r^3} - \frac{GM}{r^2}. \tag{19}$$

Eq. (19) can be derived from a potential and then from Liouville's theorem it follows that the distribution function, f, satisfies the collisionless Boltzmann equation:

$$\frac{\partial f}{\partial t} + v_r\frac{\partial f}{\partial r} + \frac{\partial f}{\partial v_r} \cdot \left[\frac{L_2}{r^3} - g(r)\right] = 0 \tag{20}$$

Assuming a non-zero cosmological constant, Eq. (19) becomes:

$$\frac{dv_r}{dt} = -\frac{GM}{r^2} + \frac{L^2(r)}{M^2r^3} + \frac{\Lambda}{3}r \tag{21}$$

(Peebles 1993; Bartlett & Silk 1993; Lahav 1991; Del Popolo & Gambera 1998, 1999). Integrating Eq. (21) we have:

$$\frac{1}{2}\left(\frac{dr}{dt}\right)^2 = \frac{GM}{r} + \int \frac{L^2}{M^2r^3}dr + \frac{\Lambda}{6}r^2 + \epsilon, \tag{22}$$

where the value of the specific binding energy of the shell, ϵ, can be obtained using the condition for turn-around, $\frac{dr}{dt} = 0$. In turn the binding energy of a growing mode solution is uniquely given by the linear overdensity, δ_i, at time t_i. From this overdensity, using the linear theory, we may obtain the binding energy for the turn-around epoch and then – for the collapse. We find the binding energy of the shell, C, using the relation between v and δ_i for the growing mode (Peebles 1980) in Eq. (22) and finally the linear overdensity at the time of collapse given by:

$$\delta_{\rm c} = \delta_{\rm co}\left[1 + \int_{r_{\rm i}}^{r_{\rm ta}} \frac{r_{\rm ta}L^2 \cdot {\rm d}r}{GM^3r^3} + \Lambda\frac{r_{\rm ta}r^2}{6GM}\right] \simeq \delta_{\rm co}\left[1 + \frac{\beta_1}{\nu^{\alpha_1}} + \frac{\Omega_\Lambda\beta_2}{\nu^{\alpha_2}}\right], \tag{23}$$

where $\alpha_1 = 0.585$, $\beta_1 = 0.46$, $\alpha_2 = 0.4$ and $\beta_2 = 0.02$.